**Geoscientific
Model Development
Discussions**

A global coupled Eulerian-Lagrangian model and 1 × 1 km CO_2 surface flux dataset for high-resolution atmospheric CO_2 transport simulations

A. Ganshin[1], T. Oda[2,*], M. Saito[2,**], S. Maksyutov[2], V. Valsala[2], R. J. Andres[3], R. Fischer[4], D. Lowry[4], A. Lukyanov[1], H. Matsueda[5], E. G. Nisbet[4], M. Rigby[6], Y. Sawa[5], R. Toumi[7], K. Tsuboi[5], A. Varlagin[8], and R. Zhuravlev[1]

[1]Central Aerological Observatory, Dolgoprudny, Russia
[2]Center for Global Environmental Research, National Institute for Environmental Studies, Tsukuba, Japan
[3]Carbon Dioxide Information Analysis Center, Oak Ridge National Laboratory, Oak Ridge, USA
[4]Department of Geology, Royal Holloway, University of London, London, UK
[5]Meteorological Research Institute, Tsukuba, Japan
[6]Center for Global Change Science, Massachusetts Institute of Technology, Cambridge, MA, USA
[7]Department of Physics, Imperial Collage London, London, UK

[8]A.N. Severtsov Institute of Ecology and Evolution, Russia

[*]now at: Cooperative Institute for Research in the Atmosphere, Colorado State University, Fort Collins, USA/Earth System Research Laboratory, National Oceanic and Atmosphere Administration, Boulder, USA

[**]now at: LSCE, Gif Sur Yvette, France

Correspondence to: A. Ganshin (alexander.ganshin@gmail.com)

A global coupled Eulerian-Lagrangian model

A. Ganshin et al.

Title Page

Abstract	Introduction
Conclusions	References
Tables	Figures

Back | Close

Full Screen / Esc

Printer-friendly Version

Interactive Discussion

Discussion Paper | Discussion Paper | Discussion Paper | Discussion Paper

A global coupled Eulerian-Lagrangian model

A. Ganshin et al.

Abstract

We designed a method to simulate atmospheric CO_2 concentrations at several continuous observation sites around the globe using surface fluxes at a very high spatial resolution. The simulations presented in this study were performed using a Lagrangian
5 particle dispersion model coupled to a global atmospheric tracer transport model with prescribed global surface CO_2 flux maps at a 1×1 km resolution. The surface fluxes used in the simulations were prepared by assembling the individual components of terrestrial, oceanic and fossil fuel CO_2 fluxes. This experimental setup (i.e., a transport model running at a medium resolution, coupled to a high-resolution Lagrangian
10 particle dispersion model together with global surface fluxes at a very high resolution), which was designed to represent high-frequency variations in atmospheric CO_2 concentration, has not been reported at a global scale previously. Two sensitivity experiments were performed: (a) using the global transport model without coupling to the Lagrangian dispersion model, and (b) using the coupled model with a reduced res-
15 olution of surface fluxes, in order to evaluate the performance of Eulerian-Lagrangian coupling and the role of high-resolution fluxes in simulating high-frequency variations in atmospheric CO_2 concentrations. A correlation analysis between observed and simulated atmospheric CO_2 concentrations at selected locations revealed that the inclusion of both Eulerian-Lagrangian coupling and high-resolution fluxes improves the high-
20 frequency simulations of the model. The results highlight the potential of a coupled Eulerian-Lagrangian model in simulating high-frequency atmospheric CO_2 concentrations at many locations worldwide. The model performs well in representing observations of atmospheric CO_2 concentrations at high spatial and temporal resolutions, especially for coastal sites and sites located close to sources of large anthropogenic
25 emissions. While this study focused on simulations of CO_2 concentrations, the model could be used for other atmospheric compounds with known estimated emissions.

A global coupled Eulerian-Lagrangian model

A. Ganshin et al.

1 Introduction

The anthropogenic emissions of greenhouse gases could potentially change the global average temperature, leading to global warming. The latest assessment report of the Intergovernmental Panel on Climate Change (IPCC-AR4) states that climate models are capable of reproducing the temperature trends observed in recent decades if they are forced with increasing concentrations of anthropogenic greenhouse gas (IPCC, 2007). A major contributor to anthropogenic greenhouse gases in the atmosphere is carbon dioxide (CO_2), which plays a key role in the global climate. Consequently, estimations of CO_2 emissions are important in assessing its influence on ongoing climate change. To understand the nature of CO_2 cycling between the land, atmosphere and ocean, it is necessary to calculate precisely the natural and anthropogenic fluxes of CO_2 and the temporal and spatial variability of CO_2 concentrations in the atmosphere.

Variations in CO_2 concentrations in the atmosphere are generally assessed using transport models with prescribed surface fluxes. Such modelling efforts are essential in order to inversely estimate the CO_2 fluxes between the atmosphere and land-ocean surfaces using model-predicted quantities of atmospheric CO_2 and corresponding observations (Gurney et al., 2002). The essential elements required for modelling of atmospheric CO_2 concentrations are a transport model, meteorological drivers, and surface fluxes. Consequently, the accuracy of simulated concentrations is strongly dependent on the ability of the transport model to represent the observed variability of atmospheric CO_2 concentrations, thereby resulting in large differences in the outputs of various models (Patra et al., 2008). Therefore, the faithful representation of CO_2 concentrations in transport models is an area of active research (Patra et al., 2008). In this study, we present a novel strategy to improve the performance of a transport model by coupling two essential components of modelling, as described below.

The concentrations of atmospheric constituents and their transport are simulated using Lagrangian or Eulerian models. In Lagrangian models, the trajectories of individual particles (representing the chemical constituents of the atmosphere) are calculated by

following a predetermined atmospheric velocity. One example of a Lagrangian model is a trajectory model in which the locations of air masses are traced using an imaginary particle. Lagrangian particle dispersion models (LPDM) are typical examples of extended trajectory models that utilize multiple particles to represent turbulence, dif-
5 fusion and convection processes, in addition to the velocities of participles along trajectory paths (e.g., Thomson, 1987). LPDMs can be run forward or backward in time. Forward simulations are generally employed to calculate the transport and dispersion of tracers from point sources, whereas backward simulations are used to estimate the potential contributions of pollutants from many sites to a single location. In this case, it
10 is only necessary to perform one backward simulation from the receptor point, tracing the given number of particles back to the possible source locations. Many previous studies have employed backward trajectory analyses of atmospheric tracer transport (Seibert et al., 1994; Stohl, 1996) and have utilized Lagrangian particle dispersion models (Lin et al., 2003; Seibert et al., 2004; Stohl et al., 2005; Folini et al., 2008; Lin
15 et al., 2011).

In the case of Eulerian models, the evolution of the concentration field is described by partial differential equations and is solved numerically using finite difference approximations (Richtmyer and Morton, 1967). Such models are applied to global-scale simulations of the concentrations of atmospheric constituents and to the inverse modelling
20 of surface fluxes (Gurney et al., 2002, 2004).

Each modelling approach has its advantages and disadvantages. For example, Eulerian models reproduce the seasonal cycle of atmospheric CO_2 concentrations reasonably well, but they suffer strongly from numerical diffusion, meaning that they perform poorly in representing synoptic, super-synoptic and hourly variations. Lagrangian
25 models, in contrast, do not suffer from numerical diffusion and they perform reasonably well in reproducing synoptic and hourly variations; however, it is necessary to employ a very long backward trajectory simulation (up to 4 months or more) to reproduce the seasonal cycle. The use of a longer trajectory results in the accumulation of errors and is computationally expensive (Stohl et al., 1998).

Full Screen / Esc

Printer-friendly Version

Interactive Discussion

Given the above limitations, it is reasonable to consider a hybrid model in which a Eulerian model is run to generate the global background concentrations of atmospheric constituents, which are then used as initial conditions for a Lagrangian model (e.g., Koyama et al., 2011). In the present study, we extended the approach introduced by Koyama et al. (2011) to a high-spatial-resolution case for simulating the concentrations of atmospheric CO_2 in the same coupled Eulerian-Lagrangian modelling framework as that used in the earlier study.

Several studies have reported the advantages of using coupled Eulerian-Lagrangian models, and some have used the WRF–STILT modelling system (Nehrkorn et al., 2010) to estimate the CO_2 surface fluxes over North America (Gourdji et al., 2010). Rigby et al. (2011) outlined a method for combining information on the emissions-mole fraction sensitivity from Eulerian and Lagrangian chemical transport models, for use in estimating emissions. Previous studies have also suggested the use of high-resolution coupled Eulerian-Lagrangian models, especially for regional-scale studies. For instance, Trusilova et al. (2010) presented a coupled TM3-STILT model simulations based on the nested atmospheric inversion scheme developed by Rodenbeck et al. (2009).

In the present study, we coupled a Eulerian model (National Institute for Environmental Studies-Transport Model, herein NIES-TM; Maksyutov et al., 2008, Belikov et al., 2011) and a Lagrangian particle dispersion model (FLEXPART; Stohl et al., 2005). We did not adopt the spatial coupling employed by similar models described above; instead, we implemented a coupling at temporal boundaries. The coupled model is described in detail in Sect. 2.

A goal of this study is to demonstrate the merit of using a coupled model together with a newly developed high-resolution (1×1 km) global CO_2 flux dataset in simulating high-frequency variations of observed atmospheric CO_2 concentrations. The use of 1-km surface fluxes combined with low-resolution meteorological wind fields for driving the model is justified because the wind fields are expected to be in a state of well-mixed daytime conditions, especially for observation sites located in relatively flat areas, where large-scale geostrophic motions are generally expected to be dominant.

A global coupled Eulerian-Lagrangian model

A. Ganshin et al.

Back | Close

Full Screen / Esc

Printer-friendly Version

Interactive Discussion

A spatial radius of correlation on the order of 100 km or more is a commonly observed feature of wind and temperature fields (Buell, 1960, 1972; Gandin, 1965).

The remainder of this paper is organised as follows. The model, data and methods are described in Sect. 2, and CO_2 emissions data and observations are presented in Sect. 3. The model results and a discussion are presented in Sect. 4, and the conclusions are provided in Sect. 5.

2 Model and methods

2.1 Lagrangian-Eulerian coupled model

Here, we describe the principles of the proposed Lagrangian-Eulerian coupled model. The concentration simulated by the Lagrangian model at the receptor (observation location) is usually calculated as the integral of the residence time of all particles at each grid cell multiplied by the flux corresponding to that grid (Lin et al., 2003; Seibert et al., 2004). The concentration of CO_2 in the Lagrangian model at any receptor point (corresponding to an observation site) can be written as follows (Holzer et al., 2000; Lin et al., 2003):

$$C(\boldsymbol{x}_r, t_r) = \int_{t_0}^{t_r} dt \int_V dV I\left(\boldsymbol{x}_r, t_r | \boldsymbol{x}, t\right) S(\boldsymbol{x}, t) + \int_V dV I\left(\boldsymbol{x}_r, t_r | \boldsymbol{x}, t_0\right) C(\boldsymbol{x}, t_0) \quad (1)$$

where: $C(\boldsymbol{x}_r, t_r)$ – concentration at receptor point $\boldsymbol{x}_r$ at time t_r; $C(\boldsymbol{x}, t_0)$ – initial concentration field at time t_0, which is obtained from the background fields simulated by the Eulerian model; $I\left(\boldsymbol{x}_r, t_r | \boldsymbol{x}, t\right)$ – influence function or Green's function linking sources and sinks $S(\boldsymbol{x}, t)$ to the concentrations; and dV – volume element. The first term of Eq. (1) denotes the concentration change at the receptor from sources/sinks in domain V during the time interval between initialization and observation. The second term refers to the contribution to the concentration at the receptor point by the advection of CO_2 from the background tracer field $C(\boldsymbol{x}, t_0)$, which is provided by a Eulerian model. From a

Lagrangian viewpoint, the influence function corresponds to the transition probability $p(x_r, t_r | x, t)$ along the air mass trajectories $x_n(t)$, calculated by the Lagrangian model as follows:

$$p(x_r, t_r | x, t) = \frac{1}{N} \sum_{n=1}^{N} \delta(x_n(t) - x) \tag{2}$$

5 where: N – number of air parcels emitted in the backward direction from the receptor point, and δ – delta function representing the presence or absence of parcel i at location x. Hence, in discrete form, Eq. (1) can be written as follows:

$$C(x_r, t_r) = \frac{1}{N} \frac{T}{L} \sum_{ijk}^{IJK} \sum_{l=o}^{L} S_{ijk}^{l} \sum_{n=1}^{N} f_{ijk}^{ln} + \frac{1}{N} \sum_{ijk}^{IJK} C_{ijk}^{B} \sum_{n=1}^{N} f_{ijk}^{n} \tag{3}$$

where: i, j, k – indices of a grid cell; l – time index; C_{ijk}^{B} – initial background concen-
10 tration from the Eulerian model; f_{ijk}^{n} – 1 (parcel inside the i, j, k cell), 0 (parcel outside the i, j, k cell); T – duration of trajectories; and L – number of steps when sources are sampled by trajectories.

In the case of sampling surface sources $F(x, y, t)$, we can consider their significance to a height h (e.g., 500 m, which is the typical height of the planetary boundary layer):

$$15 \quad S(x, t) = \begin{cases} \frac{F(x,y,t) m_{air}}{h \bar{\rho}(x,y,t) m_{CO_2}}, z \leq h \\ 0, z > h \end{cases} \tag{4}$$

where: m_{air} and m_{CO_2} – molar masses of air and CO_2, respectively; and $\bar{\rho}$ – average air density below h.

Finally, we obtain

$$C(x_r, t_r) = \frac{T m_{air}}{h N L \rho m_{CO_2}} \sum_{ij}^{IJ} \sum_{l=o}^{L} F_{ij}^{l} \sum_{n=1}^{N} f_{ij}^{ln} + \frac{1}{N} \sum_{ijk}^{IJK} C_{ijk}^{B} \sum_{n=1}^{N} f_{ijk}^{n} \tag{5}$$

where the left term is associated with concentrations obtained from the Lagrangian model and the right term is the background CO_2 concentration from the global Eulerian transport model.

In our coupled model, we use FLEXPART (run in backward mode) as the Lagrangian particle dispersion model and NIES-TM as the Eulerian global transport model (see the Introduction for details). The background CO_2 values on the model grid are obtained by NIES-TM. We use a 2-day length of backward transport in FLEXPART. Gloor et al. (2001) found that a period on the order of 1.5 days is the timescale over it is still possible to discern, in the mixing ratio variations, the imprint of surface fluxes on the air parcel before its arrival at an observation point. In the present case, the background CO_2 values on the model grid points were provided by NIES-TM sampled 2 days prior to the observations.

2.2 Meteorological drivers

We used FLEXPART version 8.0 adapted to using JCDAS data (Onogi et al., 2007), which are provided on model levels and a Gaussian grid (40 model levels, T106 grid). Because the original model was designed for use on a regular latitude-longitude horizontal grid ($1.25° \times 1.25°$) and on a hybrid sigma-pressure vertical grid on 40 levels, the required parameter values were obtained via bilinear horizontal interpolation at the model levels. The temporal resolution of input data is 6 hours. The numerical constraints of the model (i.e., the maximum time-step required for a smooth tracking of contributions of grid cell fluxes to the model concentrations) demand that the model time step (τ) is below h/U, where h is the size of the flux grid cells and U is the wind speed. At a wind speed of $U = 50 \, \text{km} \, \text{h}^{-1}$, we obtain $\tau = 2$, 0.2, and 0.02 h for $h = 100$, 10, and 1 km, respectively. Therefore, we used a period of 1 min as both the particle-transport time step and the flux-integration time step (i.e., T/L of Eq. 5) for the 1-km flux setup.

The input meteorological data for the NIES-TM model were taken from NCEP reanalyses with a spatial resolution of $2.5° \times 2.5°$ on pressure levels and a temporal resolution

Full Screen / Esc

Printer-friendly Version

Interactive Discussion

of 6 h. In this version of NIES-TM, the advection terms are solved by a second-order moment scheme (Prather, 1986). The implementation is documented by Belikov et al. (2011). The spatial resolution of the simulated NIES-TM background concentration, as supplied for the FLEXPART model, was $2.5° \times 2.5°$ on 15 sigma-levels; the corresponding temporal resolution was 1 h.

3 CO_2 fluxes and observations of atmospheric CO_2 concentrations

Three types of flux scenarios are commonly used in atmospheric CO_2 simulations: fossil fuel emissions, and biospheric and oceanic sources and sinks. These three fluxes collectively represent the major types of CO_2 sources and sinks. Forest fires should also be included as a component of biospheric flux. In the present simulations, however, we excluded the contribution from forest fires assuming that it is reasonably small at the present observational sites, especially for the period of analysis used in this study. The above three fluxes are typically available at a spatial resolution of $1° \times 1°$; however, this may be insufficient to represent strong, local emissions of CO_2.

In previous coupled modelling studies (e.g., Koyama et al., 2011), the surface CO_2 fluxes at $1° \times 1°$ resolution were used for simulations of global atmospheric CO_2 concentrations. However, as mentioned above, a flux dataset prepared at a high spatio-temporal resolution is sufficient for regional high-resolution simulations (Trusilova et al., 2010). In this study, we used $1° \times 1°$ fluxes for global-scale Eulerian calculations of atmospheric CO_2 concentrations, and used 1×1 km fluxes for the Lagrangian model. These contributions are combined in the coupled model, as described in the previous section. The $1° \times 1°$ fluxes used for Eulerian simulations are the same as 1-km fluxes, with the only difference being resolution; the one exception is biospheric fluxes, for which we used those prepared by Nakatsuka and Maksyutov (2009) using an optimized CASA model.

A global coupled Eulerian-Lagrangian model

A. Ganshin et al.

3.1 Technique for handling fluxes on a 1 × 1 km grid

Here, we describe technical aspects of surface flux simulations at a very high resolution. Because each of the global 1 × 1 km flux fields (e.g., biosphere, fossil and ocean fluxes) requires ~3.5 gigabytes (GB) of computer memory, it is inconvenient to operate
5 with multiple layers of data at this resolution. To reduce the memory and disk storage requirements, we propose the novel approach outlined below.

a. The 1 × 1 km surface flux fields at a given point are calculated in the model using a combination of data fields at high and medium resolutions. In the case of fossil fuel emissions, we multiply 1-km-resolution annual mean fluxes by a medium-
10 resolution (1° × 1°) spatially varying factor that represents the seasonal cycle at a monthly time scale. This factor is derived from seasonally varying fossil-fuel-emissions data (Andres et al., 2011) at a resolution of 1° × 1°, normalized to the annual mean. We use a land-cover mask at 1-km resolution to spatially redistribute the biospheric fluxes given at medium resolution and simulated separately
15 for each of the 15 vegetation types. In this way, the memory usage and computational time are reduced considerably. A description of each dataset is given in the following subsections, and a summary of the combinations of fluxes used in the simulations is given in Table 1. The flux data at each model time step are obtained by linearly interpolating between the monthly fields, except for biospheric fluxes,
20 which are provided a daily time step.

b. Even with the flux treatment outlined above, the memory requirements remained high. Consequently, we used sparse matrix storage (a method of representing matrices populated primarily with zeros; Tewarson, 1973) to reduce the memory demand for storing the anthropogenic emission field at 1-km resolution, because
25 only ~1 % of the elements in the matrix for anthropogenic emissions have non-zero values. To speed up the element search in the sparse matrix, we employed 1-dimensional lookup tables that contain indices for the first and last non-zero elements for each longitude.

Title Page

Abstract | Introduction

Conclusions | References

Tables | Figures

|◄ | ►|

◄ | ►

Back | Close

Full Screen / Esc

Printer-friendly Version

Interactive Discussion

It is possible to use the same approach for land fluxes; however, this has little effect on storage requirements because only about 30 % of the elements have non-zero values in this case. The combined application of the above two techniques (i.e., those described in a and b) reduces the memory demand to below 1.5 GB.

3.2 Fossil fuel CO_2 emissions

We used the Open source Data Inventory of Anthropogenic CO_2 emission (ODIAC) inventory as fossil fuel CO_2 emission fields, which is a global 1×1 km fossil fuel CO_2 emission inventory based on country-level fuel consumption, a global power plant database and satellite observations of nightlight (Oda and Maksyutov, 2011). National annual total CO_2 emissions were estimated using BP's fuel consumption statistics for coal, oil and natural gas (BP, 2008). The spatial distribution of point emissions was determined using power plant locations included in the CARbon Monitoring and Action (CARMA) power plant database (available at http://www.carma.org), and nightlight distributions were used for emissions from sources other than power plants. For further details of the ODIAC inventory, see Oda and Maksyutov (2011). We used US Department of Energy Carbon Dioxide Information Analysis Center (CDIAC) monthly emission inventory ($1° \times 1°$ resolution) to create monthly fields (Andres et al., 2011). The CDIAC monthly emission inventory was created using the monthly fuel consumptions of the top 21 emitting countries. For other countries, we used a proxy based on the data for the country among the top 21 with the most similar climate and economics. Further details of this approach are given in Andres et al. (2011). In the present study, the CDIAC monthly inventory was used to distribute ODIAC annual totals into the 12 months of the year. Monthly values on $1° \times 1°$ grids were divided by annual totals at the grids, yielding $1° \times 1°$ normalized coefficient fields that were applied to 1×1 km ODIAC annual fields to derive monthly varying fields. For the Eulerian model simulation, we created $1° \times 1°$ emission fields from the 1×1 km ODIAC (for the spatial pattern) and $1° \times 1°$ CDIAC (for monthly variability) inventories.

A global coupled Eulerian-Lagrangian model

A. Ganshin et al.

Full Screen / Esc

Printer-friendly Version

Interactive Discussion

3.3 Terrestrial biosphere fluxes

Vegetation CO_2 fluxes were simulated with the terrestrial biospheric model VISIT (Ito et al., 2007) at a resolution of $0.5° \times 0.5°$ and a daily time step for each of 15 vegetation types for each grid, closely following the procedure described by Saito et al. (2011), who simulated the ecosystem processes for four dominant vegetation types using medium-resolution fluxes. However, for high-resolution fluxes the number of vegetation types at each grid point (on a $0.5° \times 0.5°$ grid) should be extended to include all possible types. The fluxes were interpolated spatially to each pixel of the vegetation map. Vegetation cover was derived from the Moderate Resolution Imaging Spectroradiometer (MODIS) Land Cover Product (Friedl et al., 2002). The present study used a global dataset in the Plate Carree projection (IGBP vegetation classification) at 30 arcseconds (~ 1 km). This product was derived from MODIS data for the year 2001 and is based on the reprojected mosaic exports from the MODIS MOD12Q1 v.004 dataset (available at http://duckwater.bu.edu/lc/datasets.html).

MODIS-IGBP classification divides terrestrial land covers into 17 biome types and water body, whereas VISIT treats 15 biomes; consequently, the land cover classification was reconstituted to match that of VISIT algorithms (Saito et al., 2011).

3.4 Oceanic CO_2 fluxes

Oceanic fluxes were obtained from a 4D-var assimilation system based on Valsala and Maksyutov (2010). In this system, an offline biogeochemical model was driven by reanalysis ocean currents and was used to simulate the surface ocean partial pressure of CO_2 (pCO2) and air-sea CO_2 fluxes. The surface ocean pCO$_2$ in the model was constrained by ship-based observations of corresponding pCO$_2$ values and by climatological mean maps of pCO$_2$. The model employs a variational assimilation method to constrain the simulated surface ocean pCO$_2$ with reference to observations. Climatological monthly mean air-sea ocean CO_2 flux data were constructed from this assimilation system based on the period between 1996 and 2004. The air-sea CO_2 flux

A global coupled Eulerian-Lagrangian model

A. Ganshin et al.

Back | Close

Full Screen / Esc

Printer-friendly Version

Interactive Discussion

data were remapped onto a regular 1° × 1° grid. This dataset was extended to coastal areas using land–ocean mask data (∼1-km resolution) derived from the MODIS global vegetation map described above.

3.5 Atmospheric CO_2 data

5 The model results were evaluated by comparison with atmospheric CO_2 data obtained at the following continuous observation sites, representative of both polluted and background environments:

1. Fyodorovskoye tower, Russia;

2. Meteorological Research Institute (MRI) tower, Tsukuba, Japan;

10 3. Queen's Tower, Imperial College London, London, UK;

4. Royall Holloway University, Egham, London, UK.

The Fyodorovskoye site is located in the central part of western Russia, near Tver (56°27′ N, 32°55′ E), within the Central Forest State Biosphere Natural Reserve (Milyukova et al., 2002; Kurbatova et al., 2008). The reserve is located far from industrial
15 or residential areas and is therefore largely free of air pollution. The measurement tower is 29 m high and is located on a flat surface surrounded by homogenous vegetation (spruce forest). The ambient CO_2 concentrations at heights of 0.20, 1.0, 2.0, 5.0, 11.0, 15.6, 25.0, 27.6 and 29.0 m are measured by a system comprising LiCor nondispersive infrared gas analysers (Li-Cor 6262-3 and Li-Cor 6251; LI-COR, Lincoln,
20 NB, USA), a pump (KNF, Neurberger, Germany), a switching manifold, BEV-A-Line tubing, a data logger (CR23X, Campbell Scientific Inc., Logan, UT, USA) and a laptop. The instrument was calibrated weekly using air of known CO_2 concentration (pressure bottle) and compressed pure nitrogen. CO_2 data were analysed for the year 2008.

The MRI meteorological tower, which was dismantled in 2011, was 213 m high and
25 located at MRI, Tsukuba, Japan (36°04′ N, 140°07′ E). Ambient air was introduced from

inlets installed at heights of 1.5, 25, 100 and 200 m using diaphragm air pumps, and the CO_2 concentration was measured using a non-dispersive infrared analyser (NDIR) (Inoue and Matsueda, 1996, 2001). Calibration was performed every 3 h using four standard gases (330, 360, 400 and 450 ppm) in the MRI87 scale, which is compara-
5 ble to the World Meteorological Organization (WMO) mole-fraction scale (Ishii et al., 2004). In this study, we analysed hourly data on CO_2 concentrations obtained at 200 m height for the year 2009. Hourly CO_2 concentrations were calculated by averaging the observations taken at 16-min intervals.

The other two measurement sites, Queen's Tower and Royall Holloway University of
10 London, are located within 28 km of each other (Rigby et al., 2008). The Queen's Tower (height 80 m) is located on the Imperial College campus in South Kensington (51°30′ N, 0°11′ W), several kilometres west of the geographical centre of London. Royal Holloway University (51°26′ N, 0°34′ W) is located just outside of the Greater London area, bordered by "green-belt" countryside to the west and south. Measurements were made
15 through a rooftop inlet located approximately 15 m above the ground. The site is ideally located to provide a "background" CO_2 mixing ratio for London, because the prevailing wind direction is from the southwest, blowing toward London. In this study, the hourly CO_2 concentration was calculated by averaging observational data sampled at 30-min intervals. We analysed data for 2006 and 2007. Table 2 lists a summary of the
20 observation stations used in this study.

4 Results and discussion

We performed several simulations using the new model and emissions scenarios: a "synthetic" test to compare the influence of low- and high-resolution fluxes on concentration simulations, sensitivity simulations with coupled and uncoupled versions of
25 the Lagrangian and Eulerian models, and sensitivity simulations with low- and high-resolution fluxes in the coupled model. The resulted are presented at continuous monitoring stations with and without filtering of seasonal-scale variability. As measures

of the correspondence between models and observations, we chose correlation coefficients and the centred root-mean-square difference (calculated over a 1-yr period). The Fisher r-to-z transformation was used to obtain two-tailed p-values and to assess the statistical significance of the differences between correlation coefficients.

4.1 "Synthetic" test

To demonstrate the differences between the usage of low- and high-resolution CO_2 fluxes, we performed a "synthetic" test that examined the transport of CO_2 around the city of Moscow, where several large power plants are located, emitting strong plumes of CO_2 that are transported to the east of the city by winds. We selected three prospective observation sites (separated from each other by ~50 km) located east of Moscow and performed the calculations. The model results for the three sites are shown in Fig. 1a and b. For fluxes at a resolution of $1° \times 1°$, the results are similar for all three sites. For a resolution of 1×1 km, however, the results differ among the sites, clearly showing the impact of the plumes. We note that this case study serves to demonstrate the effect of flux resolution on the model results; observation data are not available from these sites for verification of the results.

4.2 Comparison of simulated concentrations at continuous monitoring stations

To demonstrate the feasibility and advantage of very-high-resolution tracer transport simulations using the coupled Eulerian-Lagrangian approach, we chose several continuous monitoring stations and performed simulations with (a) NIES-TM, (b) the coupled model with $1° \times 1°$ fluxes and (c) the coupled model with 1×1 km fluxes.

First we present simulation results at the station Fyodorovskoye, for which we used 3-hourly samples of observations and model results for the year 2008. We performed a correlation analysis between the observed and simulated concentrations, yielding correlation coefficients of 0.40 for NIES-TM, 0.43 for the coupled model with $1° \times 1°$ fluxes, and 0.46 for the coupled model with 1×1 km fluxes. In this case, the coupled model

outperforms the Eulerian model alone, although the overall correlations are relatively weak.

Similar results were obtained for the station at Egham, London, using hourly samples of observed and modelled concentrations for the year 2007. The correlation coefficients are 0.47 for NIES-TM, 0.54 for the coupled model with $1° × 1°$ fluxes, and 0.55 for the coupled model with $1 × 1$ km fluxes. Again, the correlations are relatively weak.

Overall, the correlations between observed and simulated concentrations are not as high as we expected, possibly because the model mixed layer depth was not accurately estimated. To investigate this possibility, we restricted our analysis to observations and model results sampled at hourly intervals in the daytime, because estimations of mixed layer depth are expected to be reasonably accurate during the well-mixed daytime conditions. The data selection could also consider the wind fields and boundary layer height, but we did not perform such extensive sensitivity tests based on model meteorology. Also usage of biospheric fluxes with daily variation constrains calculation of night-time values.

In the case of daytime sampling only, we see an obvious increase in the correlation coefficients between model and observations. For example, in the case of Fyodorovskoye, the correlation coefficients are 0.65 for NIES-TM, 0.68 for the coupled model with $1° × 1°$ fluxes, and 0.735 for the coupled model with $1 × 1$ km fluxes. For Egham, the corresponding correlations are 0.66, 0.66, and 0.69, respectively.

We also compared the simulations results obtained using different duration of trajectories in the Lagrangian model. Using 7-day instead of 2-day trajectories, we obtained a minor increase in the correlation coefficient from 0.735 to 0.740 for the $1 × 1$ km fluxes at Fyodorovskoye. This improvement (by 0.005) is not statistically significant because the Fisher r-to-z transformation gives a two-tailed p-value of 0.7414, which is much greater than 0.05 (the result is generally considered to be statistically significant if the p-value is less than 0.05). Therefore, relatively little is gained despite the much longer computation time required for 7-day trajectories.

For the remaining stations, we considered only daytime sampling of observations. The results are presented in Table 3, and a Taylor diagram (Taylor, 2001) for all of the simulated stations is shown in Fig. 2a. The results show that the coupled model is superior to the Eulerian model alone in terms of reproducing the observations. The use of 1 × 1 km surface fluxes (instead of 1° × 1° fluxes) results in a higher correlation coefficient between simulations and observations. For most of the stations considered here, the combined model and 1 × 1 km emissions inventory resulted in an improvement in the correlation and in the centred root-mean-square (RMS) difference.

4.3 Comparison of modelled and observed high-frequency variability

The high-resolution model performs better than the low-resolution model in representing the high-frequency variability of observed concentrations. The skill of simulations of CO_2 concentrations is affected by the quality of atmospheric transport, which dominates the variability at the synoptic scale, and the accuracy of surface fluxes, which affects the seasonal cycle (Patra et al., 2008). Therefore, to evaluate the quality of high-resolution simulations it is advisable to separate the high-frequency synoptic-scale variability from the low-frequency variability related to the seasonal cycle of surface fluxes.

The high-frequency variability was extracted from the observations and from the model results by employing the following equation:

$$C_{\mathrm{d}} = C_i - \frac{1}{n+1} \sum_{j=i-n/2}^{i+n/2} C_j \qquad (6)$$

where: C_{d} – de-seasonalized CO_2 concentration; C_i – original CO_2 concentration; and C_j – average CO_2 concentration over a 30-day period. Fifteen-day averaging was performed at the beginning and end of the analysis period.

Table 4 summarizes of correlation coefficients and RMS differences. The results for individual stations are shown in Figs. 3–6 for a period of 4 months. A Taylor diagram (Taylor, 2001) is presented in Fig. 2b. The coupled model outperforms the Eulerian

model for all stations. The use of 1×1 km fluxes further improves the correlations and the RMS differences, although in some cases there is no clear advantage over the use of $1° \times 1°$ fluxes. For the site at Fyodorovskoye and the MRI tower, the correlations are relatively weak for all flux resolutions, possibly due to seasonal variations (which could potentially affect the total correlation).

5 Conclusions

We demonstrated the feasibility of a very-high-resolution tracer transport simulation with a coupled Eulerian-Lagrangian model extended to a global flux-field resolution of 1×1 km. We prepared and tested a high-resolution flux dataset and model framework, and performed simulations of atmospheric CO_2 at selected observational points using (a) a grid-based Eulerian transport model running at a medium resolution of $2.5°$, (b) a Lagrangian plume dispersion model and (c) surface fluxes at a resolution of 1×1 km. A comparison of modelled and observed CO_2 simulations revealed that the coupled model outperforms the Eulerian model alone. The use of surface fluxes at a resolution of 1×1 km has a clear advantage over lower-resolution ($1° \times 1°$) fluxes in reproducing the high-concentration spikes caused by anthropogenic emissions. We propose a technique to represent fluxes as a combination of fixed spatial patterns at a high resolution and temporal variability at medium resolution, thereby significantly reducing memory and computational demands. This model can be efficiently used to analyse continuous observation data for sites downwind of a large emitting source. The model explicitly treats areas of sharp discontinuities in CO_2 flux, such as coastlines, where many background monitoring sites are located. It is also possible to use the model to simulate and analyse observations from satellites and aircraft, and to perform inverse modelling and validation of high-resolution emission datasets.

References

Andres, R. J., Gregg, J. S., Marland, G., and Boden, T. A.: Monthly, global emissions of carbon dioxide from fossil fuel consumption, Tellus B, 63(3), 309–327, 2011.

Belikov, D., Maksyutov, S., Miyasaka, T., Saeki, T., Zhuravlev, R., and Kiryushov, B.: Mass-conserving tracer transport modelling on a reduced latitude-longitude grid with NIES-TM, Geosci. Model Dev., 4, 207–222, doi:10.5194/gmd-4-207-2011, 2011.

BP: Statistical Review of World Energy, London, available at: http://www.bp.com/productlanding.do?categoryId=6929&contentId=7044622 (last access: 23 August 2010), 2008.

Buell, C. E.: The structure of two-point wind correlations in the atmosphere, J. Geophys. Res., 65(10), 3353–3366, 1960.

Buell, C. E.: Correlation functions for wind and geopotential on isobaric surfaces, J. Appl. Meteor., 11, 51–59, 1972.

Core Writing Team: Pachauri, R. K. and Reisinger, A. (Eds.): IPCC Fourth Assessment Report (AR4): Climate Change 2007: Synthesis Report: Contribution of Working Groups I, II and III to the Fourth Assessment Report of the Intergovernmental Panel on Climate Change, IPCC, Geneva, Switzerland, 104, 2007.

Folini, D., Ubl, S., and Kaufmann, P.: Lagrangian particle dispersion modeling for the high Alpine site Jungfraujoch, J. Geophys. Res., 113, D18111, doi:10.1029/2007JD009558, 2008.

Friedl, M. A., McIver, D. K., Hodges, J. C. F., Zhang, X. Y., Muchoney, D., Strahler, A. H., Woodcock, C. E., Gopal, S., Schneider, A., Cooper, A., Baccini, A., Gao, F., and Schaaf, C.: Global land cover mapping from MODIS: Algorithms and early results, Remote Sens. Environ., 83(1–2), 2870-302, 2002.

A global coupled Eulerian-Lagrangian model

A. Ganshin et al.

Title Page

Abstract	Introduction
Conclusions	References
Tables	Figures

◄ | ►►

◄ | ►

Back | Close

Full Screen / Esc

Printer-friendly Version

Interactive Discussion

Gandin, L. S.: Objective analysis of meteorological fields, Translation US Dep. Commerce, Springfield, Va., 242 pp., 1965.

Gloor, M., Bakwin, P., Hurst, D., Lock, L., Draxler, R., and Tans P.: What is the concentration footprint of a tall tower?, J. Geophys. Res., 106(D16), 17831–17840, 2001.

Gourdji, S. M., Hirsch, A. I., Mueller, K. L., Yadav, V., Andrews, A. E., and Michalak, A. M.: Regional-scale geostatistical inverse modeling of North American CO_2 fluxes: a synthetic data study, Atmos. Chem. Phys., 10, 6151–6167, doi:10.5194/acp-10-6151-2010, 2010.

Gurney, K. R., Law, R. M., Denning, A. S., Rayner, P. J., Baker, D., Bousquet, P., Bruhwiler, L., Chen, Y.-H., Ciais, P., Fan, S., Fung, I. Y., Gloor, M., Heimann, M., Higuchi, K., John, J., Maki, T., Maksyutov, S., Masarie, K., Peylin, P., Prather, M., Pak, B. C., Randerson, J., Sarmiento, J., Taguchi, S., Takahashi, T., and Yuen, C.-W.: Towards robust regional estimates of CO_2 sources and sinks using atmospheric transport models, Nature, 415, 626–630, 2002.

Gurney, K. R., Scott Denning, A., Rayner, P., Pak, B., Baker, D., Bousquet, P., Bruhwiler, L., Chen, Y.-H., Ciais, P., Fung, I. Y., Heimann, M., Higuchi, K., John, J., Maki, T., Maksyutov, S., Peylin, P., Prather, M., and Taguchi, S.: Transcom 3 inversion intercomparison: Model mean results for the estimation of seasonal carbon sources and sinks, Global Biogeochem. Cy., 18, GB1010, doi:10.1029/2003GB002111, 2004.

Holzer, M. and Hall, T. M.: Transit-time and tracer-age distributions in geophysical flows, J. Atmos. Sci., 57, 3539–3558, 2000.

Inoue, H. Y. and Matsueda, H.: Variations in atmospheric CO2 at the Meteorological Research Institute, Tsukuba, Japan, J. Atmos. Chem., 23, 137–161, 1996.

Inoue, H. Y. and Matsueda, H.: Measurements of atmospheric CO_2 from a meteorological tower in Tsukuba, Japan, Tellus, 53B, 205–219, 2001.

Ishii, M., Saito, S., Tokieda, T., Kawano, T., Matsumoto, K., and Yoshikawa-Inoue, H.: Variability of Surface Layer CO_2 Parameters in the Western and Central Equatorial Pacific, Global Environmental Changes in the Ocean and on Land, 59–94, 2004.

Ito, A., Inatomi, M., Mo, W., Lee, M., Koizumi, H., Saigusa, N., Murayama, S., and Yamamoto, S.: Examination of model-estimated ecosystem respiration by use of flux measurement data from a cool-temperate deciduous broad-leaved forest in central Japan, Tellus B, 59, 616–624, 2007.

Koyama, Y., Maksyutov, S., Mukai, H., Thoning, K., and Tans, P.: Simulation of variability in atmospheric carbon dioxide using a global coupled Eulerian – Lagrangian transport model, Geosci. Model Dev., 4, 317–324, doi:10.5194/gmd-4-317-2011, 2011.

A global coupled Eulerian-Lagrangian model

A. Ganshin et al.

Kurbatova, J., Li, C., Varlagin, A., Xiao, X., and Vygodskaya, N.: Modeling carbon dynamics in two adjacent spruce forests with different soil conditions in Russia, Biogeosciences, 5, 969–980, doi:10.5194/bg-5-969-2008, 2008.

Lin, J. C., Gerbig, C., Wofsy, S. C., Andrews, A. E., Daube, B. C., Davis, K. J., and Grainger, C. A.: A near-field tool for simulating the upstream influence of atmospheric observations: The Stochastic Time-Inverted Lagrangian Transport (STILT) model, J. Geophys. Res., 108(D16), 4493, doi:10.1029/2002JD003161, 2003.

Lin, J. C., Brunner, D., and Gerbig, C.: Studying Atmospheric Transport Through Lagrangian Models, EOS, 92(21), 177–184, 2011.

Maksyutov, S., Patra, P. K., Onishi, R., Saeki, T., and Nakazawa, T.: NIES/FRCGC Global Atmospheric Tracer Transport Model: Description, Validation, and Surface Sources and Sinks Inversion, J. Earth Simul., 9, 3–18, 2008.

Milyukova, I. M., Kolle, O., Varlagin, A. V., Vygodskaya, N. N., Schulze, E. D., and Lloyd, J.: Carbon balance of a southern taiga spruce stand in european Russia, Tellus B, 54, 429–442, 2002.

Nakatsuka, Y. and Maksyutov, S.: Optimization of the seasonal cycles of simulated CO2 flux by fitting simulated atmospheric CO_2 to observed vertical profiles, Biogeosciences, 6, 2733–2741, doi:10.5194/bg-6-2733-2009, 2009.

Nehrkorn, T., Eluszkiewicz, J., Wofsy, S. C., Lin, J. C., Gerbig, C., Longo, M., and Freitas, S.: Coupled weather research and forecasting-stochastic time-inverted lagrangian transport (WRF–STILT) model, Meteorol. Atmos. Phys., 107(1–2), 51–64, doi:10.1007/s00703-010-0068-x, 2010.

Oda, T. and Maksyutov, S.: A very high-resolution (1 km × 1 km) global fossil fuel CO_2 emission inventory derived using a point source database and satellite observations of nighttime lights, Atmos. Chem. Phys., 11, 543–556, doi:10.5194/acp-11-543-2011, 2011.

Onogi, K., Tsutsui, J., Koide, H., Sakamoto, M., Kobayashi, S., Hatsushika, H., Matsumoto, T., Yamazaki, N., Kamahori, H., Takahashi, K., Kadokura, S., Wada, K., Kato, K., Oyama, R., Ose, T., Mannoji, N., and Taira, R.: The JRA-25 Reanalysis, J. Meteor. Soc. Japan, 85, 369–432, 2007.

Patra, P. K., Law, R. M., Peters, W., Rodenbeck, C., Takigawa, M., Aulagnier, C., Baker, I., Bergmann, D. J., Bousquet, P., Brandt, J., Bruhwiler, L., Cameron-Smith, P. J., Christensen, J. H., Delage, F., Denning, A. S., Fan, S., Geels, C., Houweling, S., Imasu, R., Karstens, U., Kawa, S. R., Kleist, J., Krol, M. C., Lin, S.-J., Lokupitiya, R., Maki, T., Maksyutov, S., Niwa,

Y., Onishi, R., Parazoo, N., Pieterse, G., River, L., Satoh, M., Serrar, S., Taguchi, S., Vautard, R., Vermeulen, A. T., and Zhu, Z.: TransCom model simulations of hourly atmospheric CO_2: Analysis of synoptic-scale variations for the period 2002–2003, Global Biogeochem. Cy., 22, GB4013, doi:10.1029/2007GB003081, 2008.

5 Richtmyer, R. D. and Morton, K. W.: Difference Methods for Initial-Value Problems, 2nd Edn., Wiley-Interscience, 1967.

Rigby, M., Manning, A. J., and Prinn, R. G.: Inversion of long-lived trace gas emissions using combined Eulerian and Lagrangian chemical transport models, Atmos. Chem. Phys. Discuss., 11, 14689–14717, doi:10.5194/acpd-11-14689-2011, 2011.

10 Rigby, M., Toumi, R., Fisher, R., Lowry, D., and Nisbet, E. G.: First continuous measurements of CO_2 mixing ratio in central London using a compact diffusion probe, Atmos. Environ, 42, 8943–8953, 2008.

Rödenbeck, C., Gerbig, C., Trusilova, K., and Heimann, M.: A two-step scheme for high-resolution regional atmospheric trace gas inversions based on independent models, Atmos.
15 Chem. Phys., 9, 5331–5342, doi:10.5194/acp-9-5331-2009, 2009.

Saito, M., Ito, A., and Maksyutov, S.: Evaluation of Biases in JRA-25/JCDAS precipitation and their Impact on the Global Terrestrial Carbon Balance, J. Clim., 21, 4109–4125, doi:10.1175/2011JCLI3918.1, 2011.

Seibert, P. and Frank, A.: Source-receptor matrix calculation with a Lagrangian particle disper-
20 sion model in backward mode, Atmos. Chem. Phys., 4, 51–63, doi:10.5194/acp-4-51-2004, 2004.

Seibert, P., Kromp-Kolb, H., Baltensperger, U., Jost, D.T., Schwikowski, M., Kasper, A., and Puxbaum, H.: Trajectory analysis of aerosol measurements at high Alpine sites, edited by: Borrell, P M., Borrell, P., Cvitas, T., and Seiler, W., Proceedings of the EUROTRAC Sympo-
25 sium '94 SPB Academic Publishing, Hague, 1283, 689–693, 1994.

Stohl, A.: Trajectory statistics – a new method to establish source-receptor relationships of air pollutants and its application to the transport of particulate sulphate in Europe, Atmos. Environ., 30, 579-587, 1996.

Stohl, A.: Computation, accuracy and applications of trajectories – review and bibliography,
30 Atmos. Environ., 32(6), 947–966, 1998.

Stohl, A., Forster, C., Frank, A., Seibert, P., and Wotawa, G.: Technical note: The Lagrangian particle dispersion model FLEXPART version 6.2, Atmos. Chem. Phys., 5, 2461–2474, doi:10.5194/acp-5-2461-2005, 2005.

A global coupled Eulerian-Lagrangian model

A. Ganshin et al.

Taylor, K. E.: Summarizing multiple aspects of model performance in a single diagram, J. Geophys. Res., 106, 7183–7192, 2001.

Tewarson, R. P.: Sparse matrices, Academic Press, 1973.

Trusilova, K., Rödenbeck, C., Gerbig, C., and Heimann, M.: Technical Note: A new coupled system for global-to-regional downscaling of CO_2 concentration estimation, Atmos. Chem. Phys., 10, 3205–3213, doi:10.5194/acp-10-3205-2010, 2010.

Valsala, K. V. and Maksyutov, S.: Simulation and assimilation of global ocean pCO_2 and air-sea CO_2 fluxes using ship observations of surface ocean pCO_2 in a simplified biogeochemical offline model, Tellus, 62B, 821–840, doi:10.1111/j.1600-0889.2010.00495.x, 2010.

A global coupled Eulerian-Lagrangian model

A. Ganshin et al.

Title Page

Abstract | Introduction

Conclusions | References

Tables | Figures

|◄ | ►|

◄ | ►

Back | Close

Full Screen / Esc

Printer-friendly Version

Interactive Discussion

Table 1. Combinations of emissions analysed in this study.

Type of emissions	High resolution	Low resolution
Fossil fuel	1 annual file with a resolution of 1×1 km for spatial representation	12 monthly files with a resolution of $1° \times 1°$ for temporal variations
Biosphere	Global vegetation map (15 biotypes) with a resolution of 1×1 km for spatial representation	Fluxes with a spatial resolution of $0.5° \times 0.5°$ and a temporal resolution of 1 day for each biotype
Ocean	Sea-land mask derived from a global vegetation map for the biosphere with a resolution of 1×1 km for reconstruction of the coastline	12 monthly fluxes with a resolution of $1° \times 1°$

Table 2. General information on the stations.

Station	Longitude	Latitude	Instrument height, m	Data period
Fyodorovskoye	32.9220	56.4615	27	2008
MRI, Tsukuba	140.1237	36.0526	200	2009
Queen's Tower, London	−0.1768	51.4983	80	08.2006–06.2007
Egham, London	−0.5616	51.4266	15	2006–2007

Full Screen / Esc

Printer-friendly Version

Interactive Discussion

Table 3. Information on correlation coefficients (statistical significance between correlation coefficients (for 1°: comparison between NIES-TM and 1°; for 1 km: comparison between 1° and 1 km) and two-tailed p-value between current and previous (from the cell to the left of the current cell in table) correlation coefficients)/centred root-mean-square difference between simulations and observations.

Station	NIES-TM	Coupled model (1° surface fluxes)	Coupled model (1 km surface fluxes)
Fyodorovskoye	0.65/8.6	0.68(0.11)/8.3	0.73(0.00)/7.7
MRI, Tsukuba	0.38/8.2	0.42(0.14)/8.0	0.47(0.06)/7.9
Queen's Tower, London	0.66/8.9	0.79(0.00)/7.3	0.81(0.07)/6.8
Egham, London, 2006	0.68/10.3	0.78(0.00)/9.0	0.78(0.70)/8.8
Egham, London, 2007	0.66/15.6	0.66(0.71)/15.4	0.69(0.06)/14.4

Title Page

Abstract   Introduction

Conclusions   References

Tables   Figures

◀◀   ▶▶

◀   ▶

Back   Close

Full Screen / Esc

Printer-friendly Version

Interactive Discussion

Table 4. Information on correlation coefficients (statistical significance between correlation coefficients (for 1°: comparison between NIES-TM and 1°; for 1 km: comparison between 1° and 1 km) and two-tailed p-value between current and previous (from the cell to the left of the current cell in table) correlation coefficients)/centred root-mean-square difference between simulations and observations. The results have been deseasonalized.

Station	NIES-TM	Coupled model (1° surface fluxes)	Coupled model (1 km surface fluxes)
Fyodorovskoye	0.17/6.1	0.34(0.00)/5.7	0.34(0.95)/5.7
MRI, Tsukuba	0.14/6.8	0.23(0.01)/6.8	0.33(0.00)/6.7
Queen's Tower, London	0.55/5.5	0.66(0.00)/4.9	0.69(0.06)/4.7
Egham, London, 2006	0.52/7.2	0.73(0.00)/5.8	0.71(0.21)/6.0
Egham, London, 2007	0.52/9.0	0.55(0.17)/8.7	0.63(0.00)/8.2
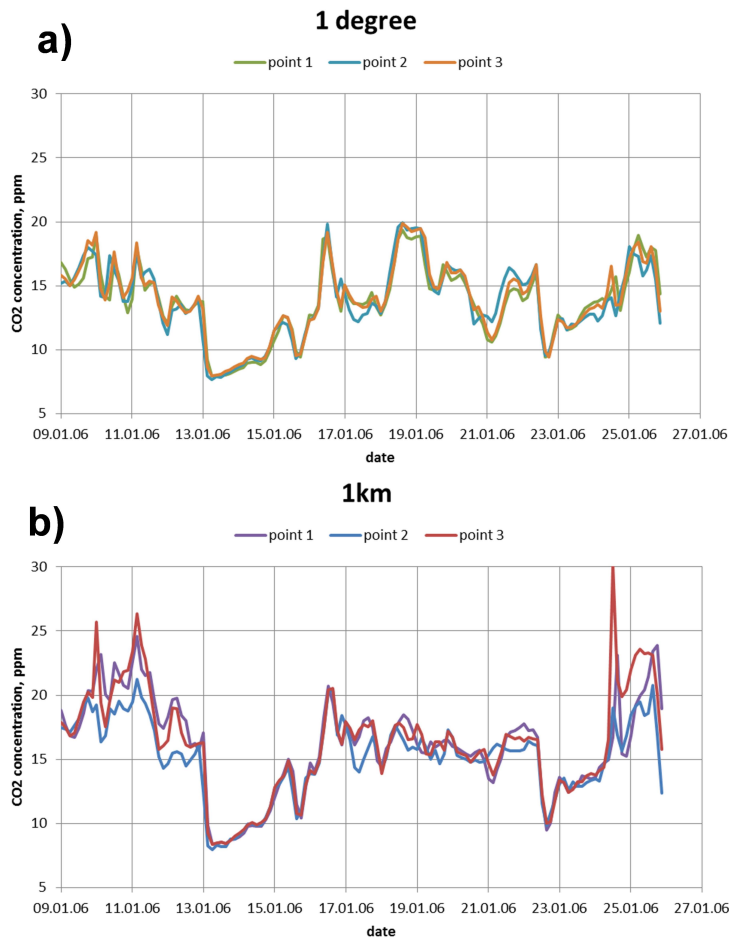
Fig. 1. Results for three imaginary observation sites located east of Moscow. **(a)** 1° resolution; **(b)** 1-km resolution.

Title Page

Abstract | Introduction

Conclusions | References

Tables | Figures

|◄ | ►|

◄ | ►

Back | Close

Full Screen / Esc

Printer-friendly Version

Interactive Discussion

Full Screen / Esc

Printer-friendly Version

Interactive Discussion
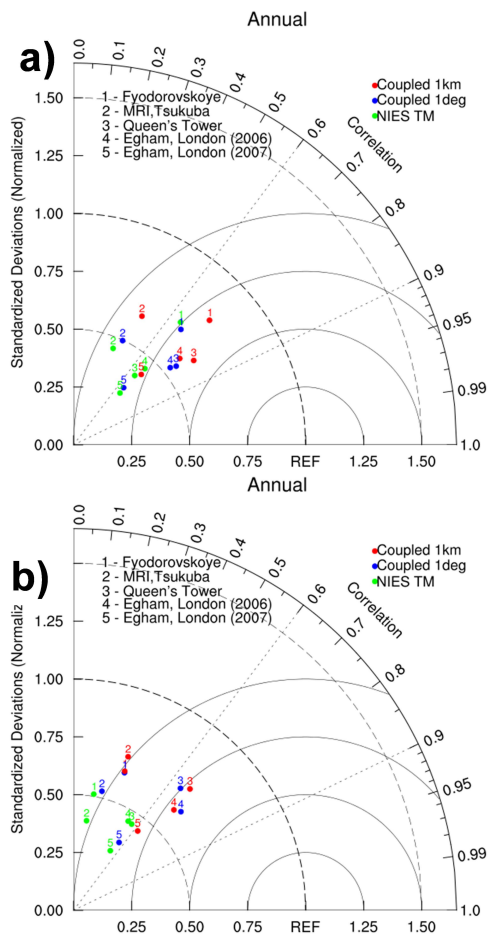
Fig. 2. Taylor diagram showing the simulated results: **(a)** without being deseasonalized; **(b)** de-seasonalized.

Full Screen / Esc

Printer-friendly Version

Interactive Discussion
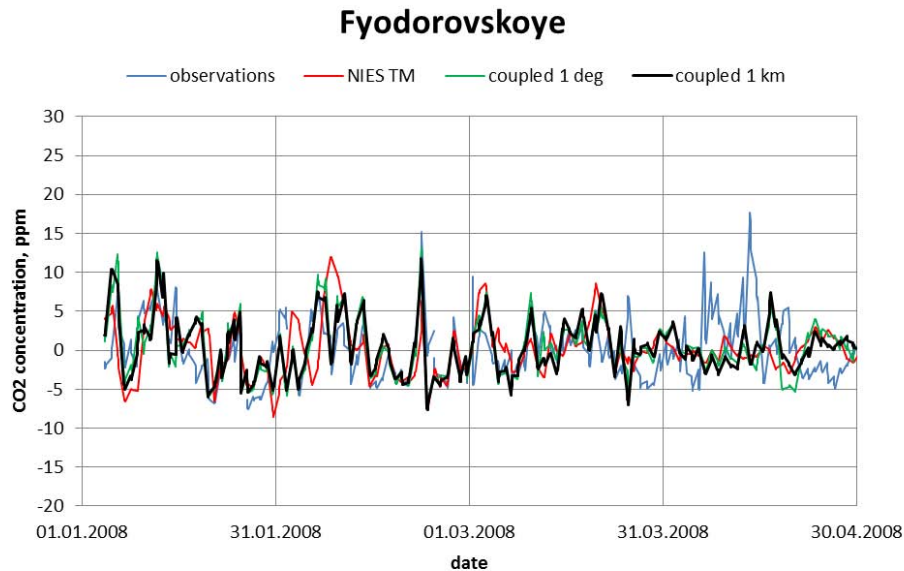
Fig. 3. Deseasonalized results for Fyodorovskoye tower (representative 4-month time series).
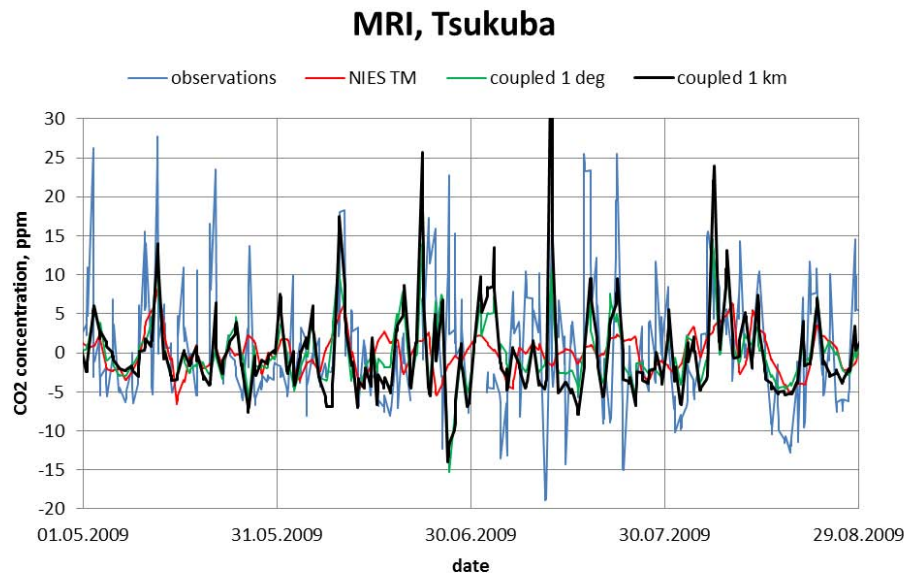
Fig. 4. Deseasonalized results for MRI tower (representative 4-month time series).
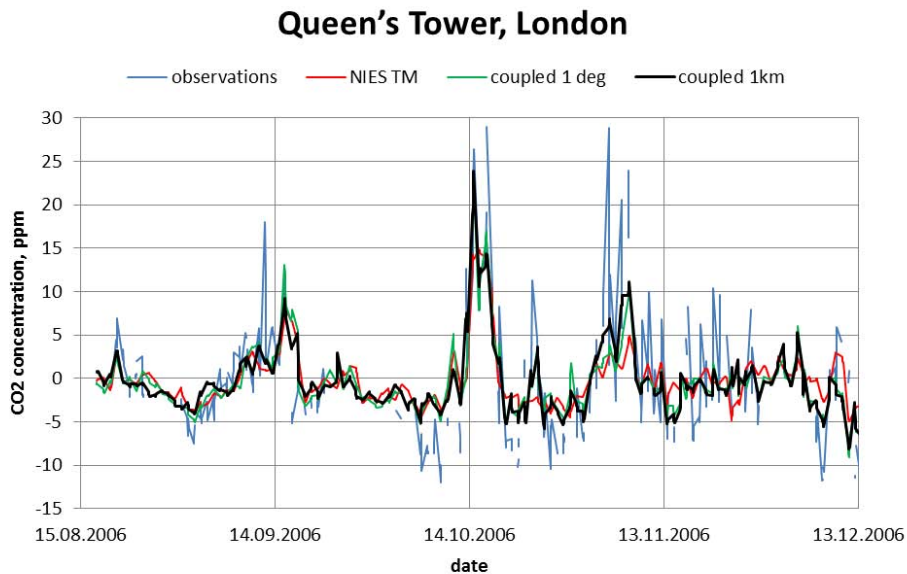
Fig. 5. Deseasonalized results for Queen's Tower, London (representative 4-month time series).
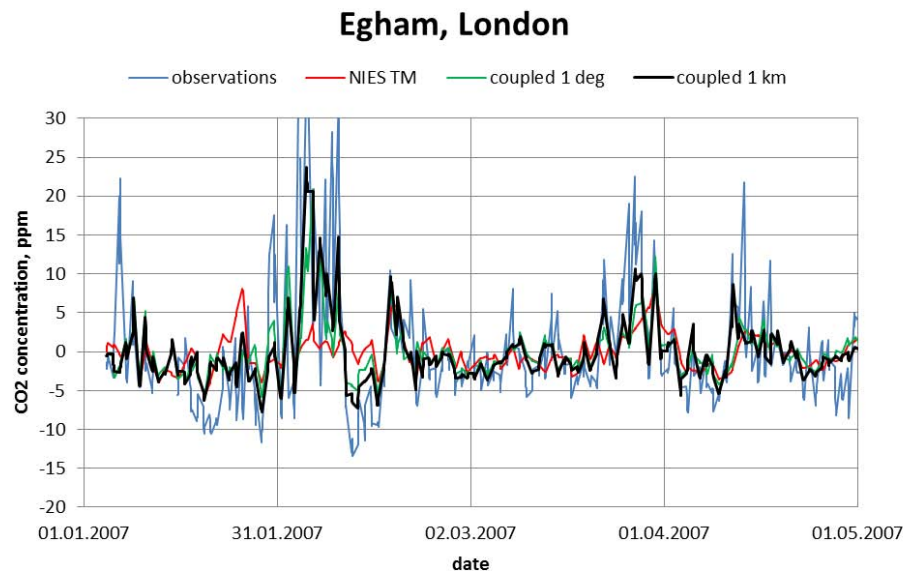
Egham, London

Fig. 6. Deseasonalized results for Egham, London (representative 4-month time series).